THE JOURNAL OF PHYSICAL CHEMISTRY

Subscriber access provided by Bibliothèque de l'Université Paris-Sud

C: Plasmonics; Optical, Magnetic, and Hybrid Materials

Understanding Solid-State Solvation-Enhanced Thermally Activated Delayed Fluorescence Using a Descriptor-Tuned Screened Range-Separated Functional

Chao Wang, and Qisheng Zhang

J. Phys. Chem. C, **Just Accepted Manuscript** • DOI: 10.1021/acs.jpcc.8b08228 • Publication Date (Web): 21 Nov 2018

ACS Publications

is published by the American Chemical Society. 1155 Sixteenth Street N.W., Washington, DC 20036

Understanding Solid-State Solvation-Enhanced Thermally Activated Delayed Fluorescence Using a Descriptor-Tuned Screened Range-Separated Functional

Chao Wang, and Qisheng Zhang**

MOE Key Laboratory of Macromolecular Synthesis and Functionalization, Department of Polymer Science and Engineering, Zhejiang University, Hangzhou 310027, China

Abstract: An efficient computational protocol suitable for both solutions and solid films can accelerate the development of efficient thermally activated delayed fluorescence (TADF) emitters aimed at practical application in organic light-emitting diodes (OLEDs). By employing the localized orbital locator (LOL), we establish an efficient descriptor-tuning methodology for the range-separated (RS) and screened range-separated (SRS)

functionals with only one single-point calculation. This scheme provides good predictions for 28 charge transfer (CT)-type TADF emitters. Moreover, in comparison to the experimental data, the scheme presents a mean absolute deviation of 0.09 eV for the absorption energies of the lowest excited singlet state ($E_{VA}(S_1)$) in polarizable continuum model (PCM) solution and 0.10 eV for the energy difference between the lowest excited singlet and triplet states (ΔE_{ST}) under static solid-state polarization. Importantly, our results indicate that a significantly polarized S_1 is key to realizing the so-called solid-state solvation-enhanced (SSSE)-TADF, which is well captured through the screened RS functionals combined with LOL-tuning (SLOL-tuning). Compared with standard ionization potential (IP)-tuning, our scheme significantly reduces the computational cost of the prediction of singlet- and triplet-transition energies for CT molecules. It also provides a reliable approach to evaluate the practical TADF character influenced by solid-state solvation in amorphous organic thin films.

1. Introduction

According to the ratio of electric exciton generation (25% singlet vs. 75% triplet),[1] the internal efficiency of conventional fluorescence organic light-emitting diodes (OLEDs) is limited into 25% because of the spin-forbidden nature of the phosphorescent transitions in heavy atom-free organic compounds. Thermally activated delayed fluorescence (TADF) molecules, also known as the E-type delayed fluorescence emitters,[2] have attracted much attention in the past several years because they have an efficient and unique ability to harvest nonemissive triplet excitons in OLEDs approaching nearly 100% internal efficiency.[3] To realize efficient reverse intersystem crossing (ISC) from the lowest excited triplet state (T_1) to the lowest excited singlet state (S_1), the energy difference between these two states (ΔE_{ST}) must be sufficiently small (< 0.2 eV).[4-9] Constructing intramolecular charge transfer (CT) is the main strategy used to minimize ΔE_{ST} because the energy of the CT excited singlet state (^{1}CT) is lower than that of any locally excited singlet state and because the singlet-triplet splitting of a CT transition can be rather small. In theoretical studies on TADF emitters, time-dependent density functional theory (TDDFT) provides a method that strikes a balance between accuracy and computational costs.[10] However, the conventional hybrid generalized gradient approximation (hGGA) functionals, such as B3LYP and PBE0, significantly underestimate the CT excitation energies.[11-12]

Recently, it has been reported that tuning the range separation parameter ω in range-separated (RS) functional can address the CT excitation issue[13-14]. The so-called IP-tuned RS functionals can provide an accurate prediction of the lowest excited singlet state ($E_{VA}(S_1)$) and energy difference between the lowest excited singlet and triplet states (ΔE_{ST}) for TADF molecules.[15-16] Despite this successful achievement, however, standard IP-tuning requires several self-consistent field (SCF) calculations at the anionic, neutral and cationic states to determine the optimal ω (ω^*). The somewhat time-consuming nature of this scheme may restrict its application, especially for relatively large molecules such as TADF emitters. Alternatively, the RS functionals can also take advantage of the descriptor-tuning methodology developed for the calculation of TADF (CT) molecules.[17-19] In an RS functional, the amount of the exact exchange is expressed as a function of the electronic interaction distance (r_{12}). The optimally tuned RS functional should afford an appropriate proportion of the Hartree-Fock (HF) exchange in each bonding or nonbonding region (different r_{12}), which can be naturally divided in the molecule according to the degree of localization (or delocalization) of the electron density. Therefore, the system-dependent ω^* can be directly determined when

the measurement of the localization (or delocalization) of each divided region is available, and the HF%-localization relationship has been pre-established.

To perform the descriptor-tuning methodology, a reasonable descriptor should be chosen first. The conventional descriptors that measure the CT character of molecules on the basis of the ground state density,[17] transition density[20-22] and excitation energy[19, 23] can hardly characterize the localization in the molecules. Intuitive wave-function analysis tools, for example, the electron localization function (ELF)[24] and localized orbital locator (LOL),[25] can be used to reveal qualitative chemical information, including atomic shells, covalent bonds and noncovalent interactions.[26-27] It is reported that noncovalent interactions between the mental cations and protein can be intuitively shown with different strength to explore the selectivity using the ELF tool.[28] Therefore, these kinetic-density-based tools can identify the localization and delocalization regions in a molecule and thus can be used to construct the descriptor for determining the ω^*.[24, 29] It has been reported that the nonempirical ELF-tuned RS functional can reliably reproduce the vertical IPs of various small organic molecules and achieve precision

approaching that of the coupled cluster single, double and perturbative triple (CCSD(T)) method.[30] Since only one single-point calculation is required to obtain the kinetic density in the tuning procedure, we can establish efficient LOL-tuning methodology for large-size TADF molecules in the gas phase and the solvation process. The approach is also applied to the screened RS functional to understand the impact of static solid-state polarization in thin films; this polarization is reported to enhance the TADF character.[31-33]

In this paper, we study $E_{VA}(S_1)$ and ΔE_{ST} of 8 representative red TADF emitters (Figure 1), whose corresponding OLED devices reach about 12.5% external quantum efficiency.[34] An efficient descriptor-tuning methodology is established for the RS functional (LOL-tuning) and screened RS functional (SLOL-tuning) with one single-point calculation. The performance of LOL-tuning and IP-tuning on the description of the $E_{VA}(S_1)$ in polarizable continuum model (PCM) solution is compared. The results are understood from the perspective of localization and delocalization errors. The influence of the static solid-state polarization on ΔE_{ST} is also investigated using the screened

LOL-tuned RS functional. The structure-property relationship for achieving static solid-state solvation-enhanced (SSSE)-TADF[35-37] is thus established. To examine the validity of the tuning scheme, the $E_{VA}(S_1)$ and ΔE_{ST} of another 20 typical TADF molecules (Figure S1) are also benchmarked by their experimental data.

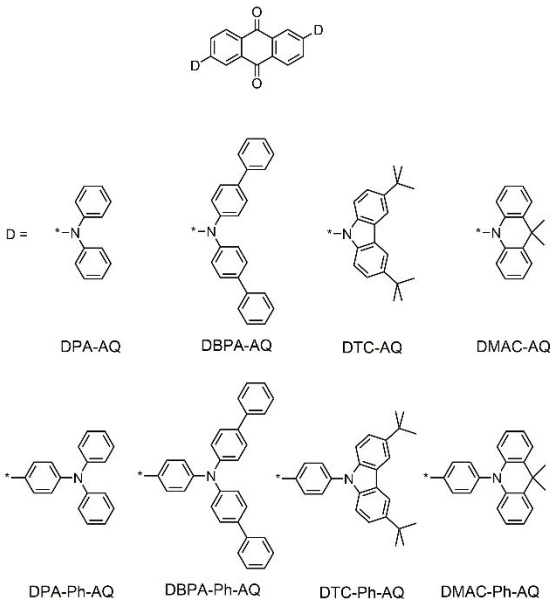

Figure 1. The representative TADF emitters studied in this work.

2. Theory and Computational Details

In an RS functional, the electron repulsion operator $1/r_{12}$ is separated into short-range (SR) and long-range (LR) parts:[38]

$$\frac{1}{r_{12}} = \frac{1-(\alpha+\beta erf(\omega r_{12}))}{r_{12}} + \frac{\alpha+\beta erf(\omega r_{12})}{r_{12}} \quad (1)$$

Thus, the exchange energy (E_X) of the RS functional is given by

$$E_x = (1-\alpha)E_{DFTx}^{SR} + \alpha E_{HF}^{SR} + (\alpha+\beta)E_{HF}^{LR} + (1-\alpha-\beta)E_{DFTx}^{LR} \quad (2)$$

E_X is dominated by a density functional theory (DFT) component in the first two terms for the SR part and a Hartree-Fock (HF) component in the next two terms for the LR part. The parameters α (< 1) and $\alpha + \beta$ (≤ 1) determine the proportion of the HF in the SR and LR, respectively. The range-separation parameter $1/\omega$ controls the electronic interaction distance (r_{12}), where the delocalized DFT exchange potential switches to the localized HF exchange.

In the solid state, the asymptotic behavior of the Coulomb potential is 1/εr via the dielectric screening effect[39-40]. Equation 2 can then be rewritten as:

$$E_x = (1-\alpha)E_{DFTx}^{SR} + \alpha E_{HF}^{SR} + (\frac{\alpha+\beta}{\varepsilon})E_{HF}^{LR} + (1-\frac{\alpha-\beta}{\varepsilon})E_{DFTx}^{LR} \quad (3)$$

where ε is the dielectric constant of the solid matrix. Because of the ω-insensitive nature of SLOL-tuning, the parameter $(\alpha+\beta)/\varepsilon$ is directly applied as the proportion of the HF component at the LR limit for describing the ΔE_{ST} under the influence of static solid-state polarization.

In the IP-tuning scheme, according to Koopmans' theorem, ω^* for an N-electron system can be nonempirically determined by minimizing [41-42]

$$J^2 = \sum_{i=0}^{1} [\varepsilon_{\mathrm{HOMO}}(N+i) + \mathrm{IP}(N+i)]^2 \tag{4}$$

where $\varepsilon_{\mathrm{HOMO}}$ is the eigenvalue of the highest occupied molecular orbital (HOMO) and IP denotes the vertical ionization potential. Since the lowest unoccupied molecular orbital (LUMO) does not correspond to the vertical electron affinity (EA), the $\varepsilon_{\mathrm{HOMO}}$ of the N+1 electron system is used instead of the LUMO.

The definition of the LOL function is as follows:[25]

$$\mathrm{LOL}(r) = \frac{t}{1+t} \tag{5}$$

$$t = \frac{\tau_0}{\tau_{\text{exact}}} \tag{6}$$

where τ_{exact} and τ_0 are the exact kinetic energy density ($(1/2)\sum_i |\nabla \varphi_i(r)|^2$) of the molecule and the kinetic energy density of the homogeneous spin-neutral electron gas ($(3/10)(3\pi^2)^{2/3}\rho(r)^{5/3}$), respectively. The LOL is a relative index in the range from 0 to 1. The lower and upper criteria indicate the extremely delocalized and localized regions, respectively.

The ground state (S_0) molecular geometries are optimized at the B3LYP/6-31G(d) level. The Tamm−Dancoff approximation (TDA) is applied to all the excited-state calculations to avoid triplet instabilities.[43-44] The lowest singlet ($E_{VA}(S_1)$) and triplet ($E_{VA}(T_1)$) vertical absorption energies are calculated using the 6-311G(d) basis set combined with the polarizable continuum model (PCM) in cyclohexane solution (ε = 2.02). The vertical single-triplet splitting is defined as $\Delta E_{VST} = E_{VA}(S_1) - E_{VA}(T_1)$. The lowest singlet ($S_1$) and triplet ($T_1$) excited-state molecular geometries are optimized at the TDA-CAM-B3LYP/6-31(d) and UCAM-B3LYP/6-31(d) levels in PCM toluene solution

(ε = 2.37). The adiabatic single-triplet splitting is defined as the energy difference between the relaxed S_1 and T_1 ($\Delta E_{AST} = E(S_1) - E(T_1)$). The LOL-, SLOL- and IP-tuned LC-ωPBE functionals refer to LC-ωPBE^{LOL}, LC-ωPBE^{SLOL} and LC-ωPBE^{IP}, respectively. IP- and LOL-tuning are performed for both the S_0 and S_1 geometries with a precision of 0.001 Bohr^{-1} for ω^*. All the DFT calculations are performed with the ultrafine grid using Gaussian 09.[45] The LOL-related calculations, natural transition orbitals (NTOs) and overlap between the hole and electron density ($\Lambda = \min[\rho^{hole}, \rho^{elec}]$) are performed using Multiwfn 3.4.[46]

3. Results and Discussion

Herein, we show the establishment of the LOL-tuning scheme. To intuitively understand the capability of the LOL to connect the localized and delocalized regions to the SR and LR distances, respectively, the percentage of the HF exchange is expressed as a function of the electronic interaction distance (r_{12}) in Figure 2a, and the electronic structure of carbazole is plotted with a color-filled LOL map in the XY molecular plane in Figure 2b. In the nonbonding region, where the LC-ωPBE^{LOL} affords a small fraction of

the HF exchange (< 25%) showing DFT-like behavior, the inner atomic shells of hydrogen, carbon and nitrogen are characterized as the strongly localized core with LOL > 0.7. At the lower limit of the bonding region, the LOL domain with edge LOL ≈ 0.5 and core LOL ≈ 1.0 is plotted around the hydrogen atom and shifted towards the carbon atom because of the typical $\sigma_{N\text{-}H}$ bond. At the upper limit of the bonding region, the π-conjugated carbon-carbon bond ($\pi_{C\text{-}C}$) is well characterized as a covalent double bond showing a somewhat concave domain with edge LOL ≈ 0.5 and core LOL ≈ 0.75. In these bonding regions, the LC-ωPBE^{LOL} affords approximately 42% to 75% HF exchange, showing mixed DFT and HF behavior. Dielectric screening in cyclohexane solution is also reflected in the LC-ωPBE^{SLOL}. According to the definition of the LOL[47] and its formula in the section of theory and computational details, the localized region (with large LOL) can be assigned to the area where the pure local DFT exchange can reproduce the exact exchange energy, and the delocalized region (with small LOL) refers to the area where the pure local DFT exchange substantially overestimates the exact exchange energy.[47] Thus, the switching between the DFT and HF components (ω^*) can be managed with the help of the localized and delocalized regions marked by

the LOL function. Our calculation indicates that the proportion of the HF exchange in the bonding and nonbonding regions is related to the LOL values.

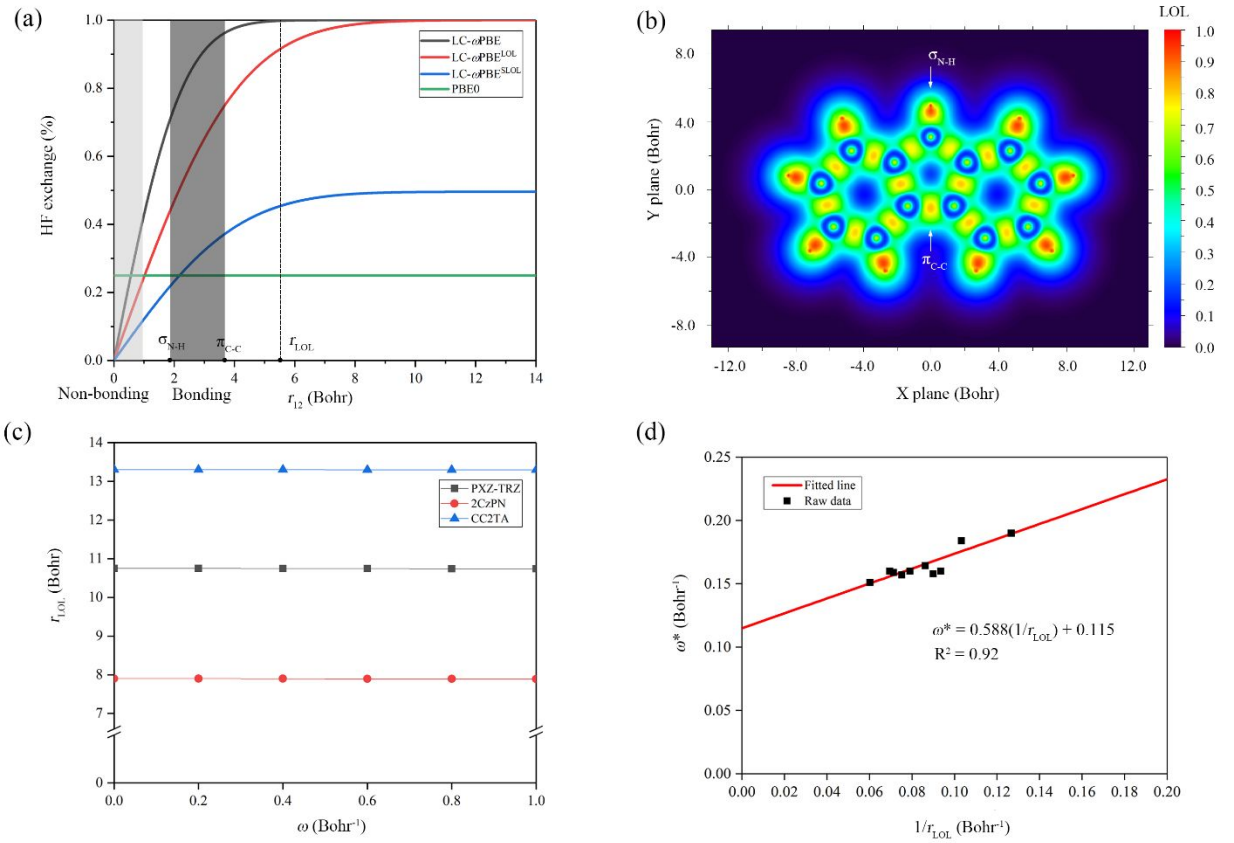

Figure 2. Establishment of the LOL-tuning scheme. (**a**) The percentage of the HF exchange as functions of r_{12} for the LC-ωPBE, PBE0, LC-ωPBE^{LOL} (ω^* = 0.221) and LC-ωPBE^{SLOL} (in cyclohexane) obtained from the calculation of carbazole. The bonding and nonbonding regions are filled with dark and light gray, respectively. (**b**) The color-

filled LOL map of carbazole in the XY plane (molecular plane). Values of zero and utility indicate significant delocalization and localization, respectively. **(c)** The r_{LOL} as a function of ω for PXZ-TRZ, 2CzPN and CC2TA calculated at the LC-ωPBE/6-31G(d) level. **(d)** The linear fitting of ω^* as a function of $1/r_{LOL}$.

Although the LOL is able to intuitively help the determination of the ω^* for localized regions, it is difficult to determine the distance in cases where the complete HF is necessary (fully delocalized region). By summing each LOL domain over the entire molecular space, the mean localization distance (r_{LOL}) can be expressed as follows:[30]

$$r_{\mathrm{LOL}} = \sqrt{\frac{\int \mathrm{LOL}(r) r^2 \mathrm{LOL}(r) dr}{\int \mathrm{LOL}(r) \mathrm{LOL}(r) dr}} \tag{7}$$

As displayed in Figure 2c, the r_{LOL} inherits the noninteracting character of the LOL function bearing the variation in the ω in the LC-ωPBE functional for different TADF molecules. Thus, the r_{LOL} can be regarded as an intrinsic molecular property for establishing the starting point of the descriptor-tuning methodology.[17, 19] Importantly, to correctly describe the CT excitation energy, the asymptotic behavior of the exchange-

correlation potential (f_{XC}) is met at r_{LOL}, where the target electron is fully delocalized because the LC-ωPBE^{LOL} affords approximately 90% HF exchange.

Although the amount of HF exchange can be expressed as a function of an inherent molecular property, i.e., the LOL domain, the problem of how to directly gauge the explicit amount of HF exchange remains unsolved. Recently, ω^* was reported to follow a quasilinear relationship with the mean ELF distance.[30] Because of the similarity between the ELF and LOL, the following relationship can be adapted:

$$\omega^* = \frac{C_1}{r_{LOL}} + C_2 \tag{8}$$

where C_1 and C_2 are the numerical constants (0.588 and 0.115, respectively) determined by the minimization of the calculated $E_{VA}(S_1)$ of 10 typical TADF training molecules (Table S1) using the experimental data of $E_{VA}(S_1)$ in cyclohexane as references (Figure 2d).[19] These model molecules have been previously studied and proven as good references in the descriptor-tuning methodology.[17, 19] A flowchart of the scheme is provided in Scheme S1. With Equation 8, we can estimate ω^* using only one

single-point calculation of the r_{LOL}. In addition, high-throughput virtual screening (HTVS) technology can take advantage of the determination procedure for ω^*, which is efficient in comparison with the previous *K*-OHF[19] and IP-tuning methodologies, as shown in Figure S2.

Now we compare the main difference between the IP-tuning and LOL-tuning. The IP-tuning is based on the density of HOMO and LUMO, while the LOL-tuning based on the total density. Therefore, the IP-tuning mainly responds to the geometric change that contributes to the HOMO and LUMO, while the LOL-tuning always responds to the geometric change. In both LC-ωPBE^{IP} and LC-ωPBE^{LOL} for different molecules in their ground states, the value of ω^* ranges from 0.143 to 0.192 Bohr^{-1}, which is obviously lower than ω = 0.4 Bohr^{-1} in the default LC-ωPBE, suggesting the importance of functional tuning (Table S2). It seems tricky that the change of ω^* from S_0 to S_1 in LC-ωPBE^{IP} is generally larger than the LC-ωPBE^{LOL}. In fact, it is not surprising because the lowest excitation usually occurs in the HOMO → LUMO transition. The ratio of the change of density to the HOMO ($\Delta\rho/\rho^{HOMO}$) is much larger than that to the total density

($\Delta\rho/\rho^{Total}$). Such insensitivity of the LOL-tuning may result in the underestimation of excitation energies. The IP-tuning scheme usually guarantees that in organic conjugated donor-acceptor molecules, the value of ω^* decreases with increasing conjugation length and saturates at long conjugation lengths.[48-50] In Equation 8, interestingly, such asymptotic behavior of the ω^* is controlled by the measurement of the total localization ($1/r_{LOL}$), and the lower limit of the ω^* is ensured by the coefficient C_2. Although both methodology is geometry-dependent, the control of such behavior is quite different.

To examine the validity of Equation 8, the general performance of LOL- and IP-tuning on the prediction of the $E_{VA}(S_1)$ of 28 typical TADF molecules (Figure S1) is assessed. As summarized in Table 1, IP-tuning exhibits reliable predictions of the $E_{VA}(S_1)$ with a mean absolute deviation (MAD) of 0.15 eV for 28 TADF emitters. Similar results are also found by Penfold (MAD of 0.09 eV for 11 TADF molecules)[16] and Sun et al. (MAD of 0.13 eV for 13 TADF molecules).[15] The MAD of 0.09 eV for the $E_{VA}(S_1)$ (0.12 eV excluding the 10 training molecules) confirms the reliability of Equation 8.

In Table 1, we notice a slight breakdown in the LC-ωPBE^{IP}, which overestimates the $E_{VA}(S_1)$ by an average of 0.25 eV (twice the MAD) for a series of three phenyl-anthraquinone (AQ)-based molecules named DPA-Ph-AQ, DBPA-Ph-AQ and DTC-Ph-AQ (Figure 1). In contrast, it performs relatively well on the analogues without a phenyl bridge between the N-donor and AQ moiety. The CT issue of TDDFT closely corresponds to the localization or delocalization error in the density functionals.[51] In particular, the total energy of a molecule should afford a linear variation bearing the change in the fractional electron number between the integer electron numbers in the exact Kohn−Sham theory.[52] Taking the case of DBPA-Ph-AQ as an example (Figure 3a), the convex behavior of the PBE0 curve indicates excessive delocalization (delocalization error), whereas the concave behavior of the LC-ωPBE curve indicates excessive localization (localization error). Both LC-ωPBE^{IP} and LC-ωPBE^{LOL} afford nearly straight lines, indicating a significant reduction in localization error compared with that of the LC-ωPBE. Since it is difficult to examine the linearity with the naked eye, the deviations in the curves from straight lines are plotted in Figure 3b. Because of the imbalanced description of the cationic and anionic state of DBPA-Ph-AQ, a small

localization error is observed for the LC-ωPBE^{IP} in the electron-deficient ($\Delta N < 0$) regime, and a slight delocalization error is observed for the LC-ωPBE^{LOL} in the electron-rich regime ($\Delta N > 0$). Subsequently, the more tightly bounded excited-state density of S_1 is obtained from the LC-ωPBE^{IP}, showing hybrid locally excited (LE) and CT character ($\Lambda = 0.33$) in comparison with the pure CT character predicted by the LC-ωPBE^{LOL} ($\Lambda = 0.20$) in Figure 3c. This difference is more pronounced in the case of DTC-Ph-AQ, where LC-ωPBE^{IP} predicts pure LE excitation for the lowest absorption (Figure S3). In Figure S4, a more balanced description is observed for DBPA-AQ. Thus, the successful prediction of the CT $E_{VA}(S_1)$ in the Donor-AQ series is related to the delocalization-error-free LC-ωPBE^{LOL} and LC-ωPBE^{IP}. Our results suggest that the LC-ωPBE^{IP} and LC-ωPBE^{LOL} have slight localization and delocalization errors, respectively, which can be ascribed to the slightly imbalanced description of the anionic and cationic states in the Donor-Ph-AQ series.

Table 1. Comparison of the $E_{VA}(S_1)$ (in eV) calculated at the TDA-LC-ωPBE^{LOL}/6-311G(d) and TDA-LC-ωPBE^{IP}/6-311G(d) levels in PCM cyclohexane solution with experimental data.

Compound	LC-ωPBE^{LOL}			LC-ωPBE^{IP}		Expt.[b]
	r_{LOL}[a]	ω^*	$E_{VA}(S_1)$	ω^*	$E_{VA}(S_1)$	$E_{VA}(S_1)$
PIC-TRZ	10.695	0.170	3.42	0.144	3.19	3.35
CC2TA	13.302	0.159	3.66	0.165	3.70	3.64
PXZ-TRZ	10.748	0.170	2.81	0.189	2.98	2.93
DPAC-TRZ	11.882	0.164	3.19	0.173	3.28	3.26
Cz-TRZ	10.883	0.169	3.57	0.183	3.67	3.43
Cz-TRZ2	11.252	0.167	3.25	0.181	3.38	3.22
3Cz-TRZ	14.017	0.157	3.53	0.175	3.66	3.59
BCz-TRZ	15.010	0.154	3.37	0.173	3.52	3.34
2CzPN	7.899	0.189	3.34	0.182	3.29	3.33
4CzPN[c]	9.427	0.177	2.89	0.149	2.60[e]	2.94
4CzIPN[c]	9.692	0.176	2.79	0.146	2.56[e]	2.85
4CzTPN[c]	9.827	0.175	2.56	0.151	2.38[e]	2.70
4CzTPNMe	11.010	0.168	2.52	0.146	2.34	2.67
DPA-DPS	11.122	0.168	3.66	0.171	3.68	3.61

DTPA-DPS	14.023	0.157	3.57	0.156	3.56	3.58
DTC-DPS	14.383	0.156	3.59	0.165	3.65	3.62
DMOC-DPS	12.657	0.161	3.40	0.175	3.50	3.38
PXZ-DPS	11.101	0.168	2.89	0.183	3.02	3.15
DMAC-DPS	11.909	0.164	3.12	0.176	3.22	3.39
PPZ-DPS	13.355	0.159	2.47	0.173	2.60	2.76
DPA-AQ	11.597	0.166	2.84	0.181	2.95	2.81
DBPA-AQ	15.739	0.152	2.65	0.161	2.72	2.72
DTC-AQ	15.434	0.153	2.62	0.178	2.85	2.68
DMAC-AQ	12.579	0.162	2.13	0.190	2.43	2.37
DPA-Ph-AQ	16.614	0.150	2.77	0.181	3.08	2.78
DBPA-Ph-AQ	20.791	0.143	2.66	0.173	2.98	2.73
DTC-Ph-AQ	20.744	0.143	2.94	0.178	3.17	2.96
DMAC-Ph-AQ	17.832	0.148	2.76	0.187	2.93	2.91
MAD			0.09		0.15	
RMSD			0.08		0.11	
Max Dev.			0.29		0.34	

[a]Calculated through Equation (5) at the LC-ωPBE/6-311G(d) level; [b]Adapted from Ref. [19]; [c]We find that these values are relatively lower than those found in Ref. [16] but agree with those in Ref. [15]

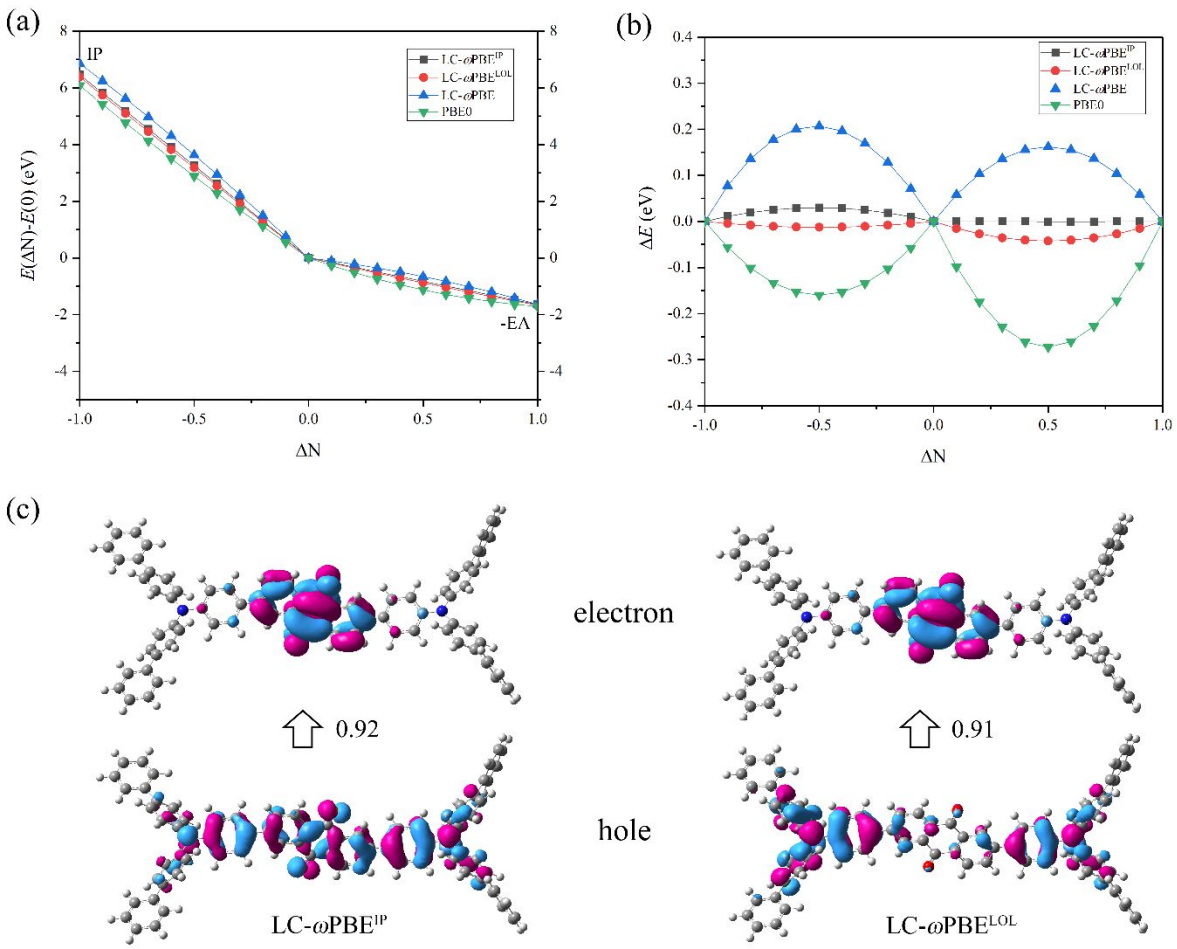

Figure 3. The impact of the delocalization and localization error. **(a)** The energy difference between the fractional charge number ($E(\Delta N)$) and the neutral charge number ($E(0)$) for DBPA-Ph-AQ. **(b)** The deviation of the curves (ΔE) from the straight lines in (a). **(c)** The distribution of the hole and electron NTOs (isovalue =0.02) of the lowest absorption with the largest weight calculated at the TDA-LC-ωPBE^{IP}/6-311G(d) and TDA-LC-ωPBE^{LOL}/6-311G(d) levels of theory in PCM cyclohexane solution.

To better understand the delocalization and localization errors in the special TADF emitters whose HOMO and LUMO significantly differ from each other, the dependence of the molecular orbital energy on the variation in the fractional electron number is investigated, as shown in Figure 4. As indicated in Janak's theorem, [53] the HOMO energy should remain constant between the integer electron numbers and be equal to the negative IPs of the system with one more electron. IP-tuning ensures that the initial slope of the total energy of the neutral system equals the negative IP.[41, 54] However, slight localization error of the HOMO is observed, leading to a slight overestimation of the HOMO-LUMO gap (Figure 3a). The conjugated phenyl ring in DBPA-Ph-AQ plays an important role because in comparison with the ring in DBPA-AQ (Figure S5), it has a vanishing influence on the LUMO and the HOMO (ω^* does not increase in DBPA-Ph-AQ.) In contrast, as shown in Figure S6, the LOL-tuning scheme ensures that the value of ω^* grows as a function of the total conjugation of the molecule (occupied orbitals) but neglects the unoccupied orbitals whose conjugation remains unchanged. As a result, overestimation of the $E_{VA}(S_1)$ is observed for the LC-ωPBE^{IP}, whereas interestingly, underestimation of the $E_{VA}(S_1)$ almost vanishes for the LC-ωPBE^{LOL}. In general, the

imbalanced description of the HOMO and LUMO, as in the case of DBPA-Ph-AQ, is inevitable in some TADF emitters because two or more donors are usually combined with only one acceptor core.[6, 55-57] We also find that the LC-ωPBE^{IP} provides a reliable calculation for the $E_{VA}(S_1)$ of 2CzPN but overestimates that of 4CzPN by approximately 0.3 eV (see also 4CzIPN, 4CzTPN and 4CzTPNMe) and that LC-ωPBE^{LOL} performs well in both situations (Table 1). Here, we highlight that the LOL-tuned RS functional can reliably describe the CT transition in TADF molecules, especially for those TADF molecules whose HOMO is much widely distributed over the molecule than the LUMO.

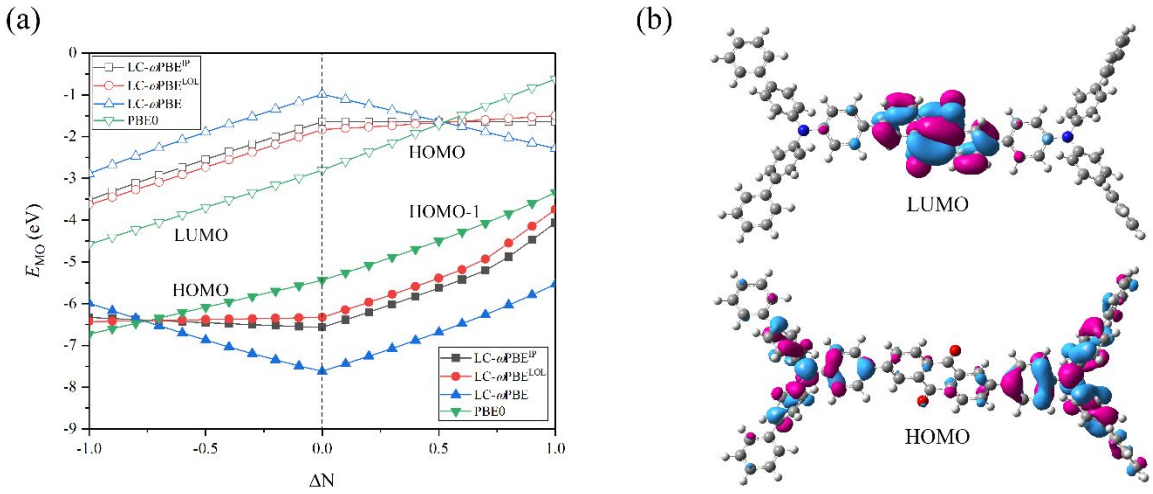

Figure 4. (a) The molecular orbital energy (E_{MO}) as a function of the fractional charge number (ΔN) in DBPA-Ph-AQ. **(b)** The corresponding distributions of the HOMO and LUMO in the neutral state.

The practical performance of TADF emitters in OLEDs depends on their ΔE_{ST} values. For the Donor-AQ and Donor-Ph-AQ TADF emitters, the calculated ΔE_{ST} in PCM solution is larger than the experimental one determined in 4,4'-bis(n-carbazolyl)-1,1'-biphenyl (CBP)-doped films (Table 2).[34] Especially for DMAC-Ph-AQ, the ΔE_{ST} values predicted by both the LC-ωPBE^{IP} and LC-ωPBE^{LOL} are substantially overestimated. The impact of the external thin film environment can be divided into two parts: (i) the impact of static solid-state polarization on the electronic structures;[58] and (ii) the impact of dynamic rearrangement and dispersion on the geometric structure, which can be addressed by combining the molecular dynamics (MD) and TDDFT calculations.[59-61] The introduction of the static dielectric screening in the LC-ωPBE^{SLOL} results in an obvious reduction in both ΔE_{VST} and ΔE_{AST} compared to those in PCM solution, indicating the obvious SSSE-TADF character. Importantly, the dynamic factor also indirectly results in the enhancement in the TADF character of these emitters by suppressing the triplet excited-state geometries with a large ΔE_{ST}.[62] Apart from the dynamic factor in the solid state, which cannot be explicitly considered with one simple calculation, we believe that static solid-state polarization is one of the main origins of the

SSSE-TADF property. In other general cases, when the ΔE_{ST} is experimentally determined from the 0-0 energy difference between S_1 and T_1 in a 77 K solvation matrix, the impact of static solid-state polarization is comparable to or even stronger than that of the dynamic factor[37, 63] because the geometric relaxation of S_1 and T_1 is generally suppressed within 0.1 eV.[15, 19] In this regard, SLOL-tuning provides an efficient approach that reflects the SSSE-TADF property. In Table S3, a more detailed comparison of the performance of IP-, LOL- and SLOL-tuning on the prediction of the ΔE_{ST} for 28 TADF molecules is explored. When LOL-tuning is employed, the MAD of the ΔE_{VST} and ΔE_{AST} is 0.13 eV and 0.10 eV, respectively. When SLOL-tuning is employed, the MAD of ΔE_{VST} is 0.10 eV in the CBP-doped film (ε = 1.73) and in cyclohexane (ε = 2.02). Additionally, we should also mention that it is difficult to perform IP-tuning or PCM-IP-tuning for a real system,[64] for example, a doped thin film, in a hybrid quantum mechanics/molecular mechanics (QM/MM) study because of the large computational demand. In contrast, the one-step SLOL-tuning scheme is capable of considering large systems.

Table 2. Comparison of the performance of LOL-, SLOL- and IP-tuning using the 6-311G(d) basis set on the prediction of the experimental ΔE_{ST} (eV) and the overlap between the hole and electron density (Λ).

Compound	LC-ωPBE^{LOL}		LC-ωPBE^{IP}		LC-ωPBE^{SLOL}				Expt.
	ΔE_{VST} (Cyc.)[a]	ΔE_{AST} (Tol.)[b]	ΔE_{VST} (Cyc.)[a]	ΔE_{AST} (Tol.)[b]	ΔE_{VST} (Cyc.)[c]	ΔE_{VST} (CBP)[c]	ΔE_{AST} (Tol.)[c]	Λ(Tol.)[c,d]	ΔE_{ST}[e]
DPA-AQ	0.53	0.56	0.56	0.56	0.47	0.47	0.38	0.26	0.29
DBPA-AQ	0.48	0.48	0.50	0.48	0.42	0.43	0.27	0.16	0.27
DTC-AQ	0.32	0.31	0.37	0.31	0.25	0.25	0.15	0.09	0.17
DMAC-AQ	0.03	0.04	0.07	0.04	0.01	0.01	0.03	0.03	0.08
DPA-Ph-AQ	0.37	0.41	0.43	0.45	0.17	0.23	0.25	0.11	0.24
DBPA-Ph-AQ	0.32	0.42	0.42	0.53	0.14	0.18	0.18	0.09	0.22
DTC-Ph-AQ	0.39	0.30	0.43	0.25	0.07	0.12	0.11	0.03	
DMAC-Ph-AQ	0.40	0.34	0.44	0.32	0.001	0.001	0.10	0.01	0.07
MAD	0.17	0.16	0.20	0.19	0.09	0.09	0.03		
RMSD	0.09	0.07	0.11	0.09	0.06	0.06	0.03		
Max Dev.	0.33	0.27	0.37	0.31	0.18	0.18	0.09		

[a] Calculated in PCM cyclohexane solution (ε = 2.02); [b] Calculated in PCM toluene solution (ε = 2.37); [c] Using the static dielectric constant of cyclohexane (ε = 2.02), toluene (ε = 2.37) and the CBP-doped thin film (ε = 1.73) experimentally determined from the relaxed Lorentz model [65];[d] The overlap between the hole and electron density is defined as min[ρ^{hole}, ρ^{elec}][46]; [e] Determined in the CBP-doped films (1 wt%);

To achieve significant SSSE-TADF, the ^{1}CT should be significantly stabilized by the solid-state solvation to have sufficient small overlap between the hole and electron density. As shown in Table 2 and Figure 5a, in the Donor-AQ series, the LC-ωPBE^{SLOL} shows a more sensitive ε-dependence of ΔE_{AST} than the LC-ωPBE^{LOL}, especially in the range from 1 to 3, because the CT state (S_1) is more easily stabilized by the polarity of the solid-state environment than the localized state (T_1) (Figure S7a). The impact of PCM solvation with increasing ε on the ΔE_{AST} is less than 0.05 eV, suggesting that the conventional solvation effect is negligible. In the Donor-Ph-AQ series (Figure 5b), the SSSE-TADF character is significantly enhanced with the decrease in Λ. In this manner, S_1 is more easily stabilized with respect to the dielectric constant than the corresponding Donor-AQ series (Figure S7b). Additionally, static solid-state polarization will also result in the complete separation of the hole and electron wave functions (Figure S8). Thus, the similar ππ* character of S_1 and T_1 gives rise to vanishing spin-

orbit coupling (SOC) between them because of the El-Sayed rule[66-67]. This highlights the importance of nonadiabatic coupling.[68-70] Consequently, a small overlap between the hole and electron density is beneficial for the SSSE-TADF property. We also suggest using the SLOL-tuning scheme, which can reflect the impact of the dielectric screening to estimate the ΔE_{ST} of the TADF emitters, especially for those emitters showing significant SSSE-TADF character. Alternative approaches, e.g., the previous *K*-OHF method (with a quasi-dielectric screening effect) [19] and IP-PCM-tuning,[32] are capable of calculating the SSSE-TADF as well.

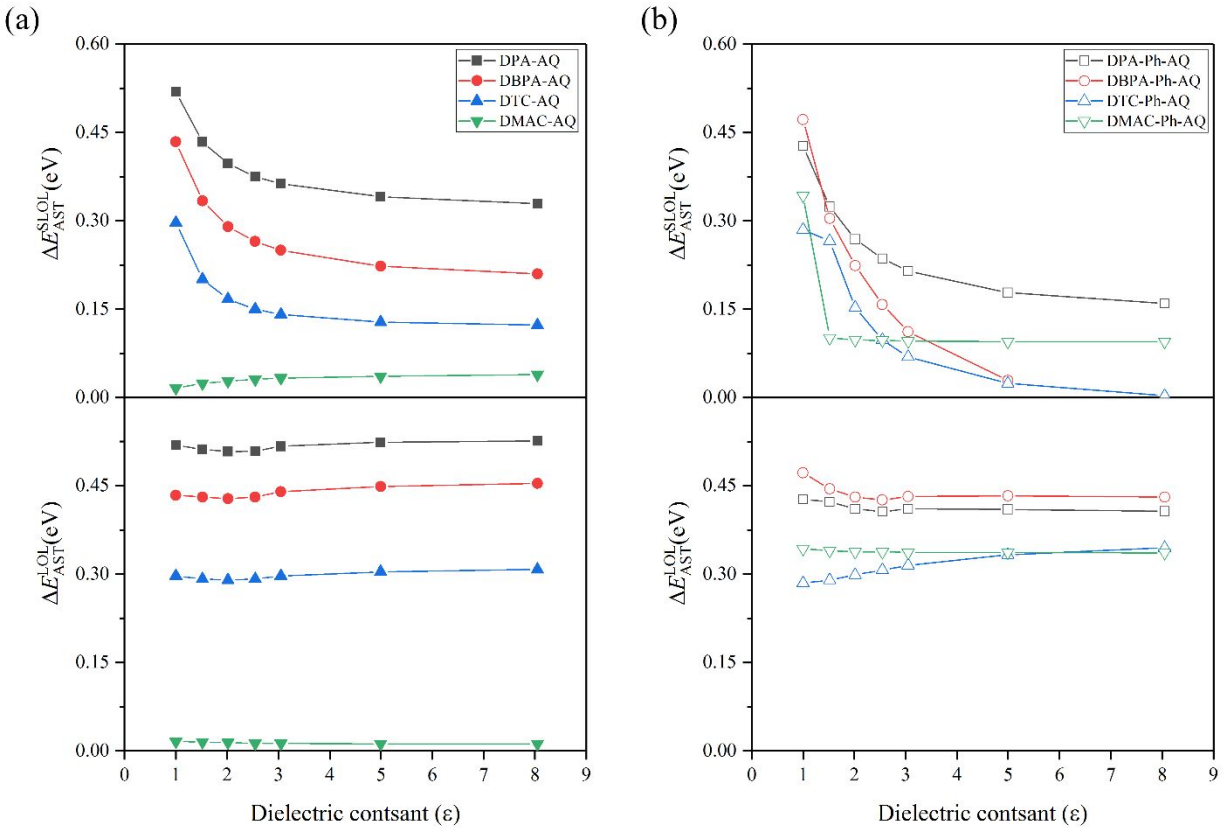

Figure 5. The E_{AST} as a function of the dielectric constant (ε) calculated at the TDA-LC-ωPBE^{LOL}/6-311G(d) level in PCM cyclohexane solution (down) and TDA-LC-ωPBE^{SLOL}/6-311G(d) (up) level for **(a)** the Donor-AQ series and **(b)** the Donor-Ph-AQ series.

4. Conclusion

In this work, we established an efficient tuning methodology using the localized orbital locator (LOL) as the descriptor with only one single-point calculation for the determination of the system-dependent optimal ω in the range-separated (RS) and screened range-separated (SRS) functionals. The $E_{VA}(S_1)$ in PCM solution and the ΔE_{ST} under solid-state polarization are well calculated using LOL-tuned RS and SRS functionals for 28 TADF emitters with MADs of 0.09 and 0.10 eV, respectively. Importantly, our results highlight that the decrease in ΔE_{ST} in organic thin films, namely, solid-state solvation-enhanced (SSSE) thermally activated delayed fluorescence (TADF), can be well reproduced by a static solid-state polarization model based on the LOL-tuned SRS functional. The S_1 state with a higher dipole moment and a smaller overlap between the hole and electron density is found to be conducive to SSSE-TADF. To accurately estimate the practical performance of TADF emitters in OLED devices, especially for those emitters with significant SSSE-TADF, we recommend using methods that can capture the dielectric screening effect for theoretical investigations.

ASSOCIATED CONTENT

Supporting Information.

The chemical structures of all TADF emitters calculated in this work, the comparison of job time of *K*-OHF, LOL- and IP-tuning schemes, the distribution of hole and electron wavefunctions of the lowest absorption of DTC-Ph-AQ using natural transition orbitals (NTOs) with the largest weight, the total energy difference of the fractional charge number ($E(\Delta N)$) to the neutral one ($E(0)$) for DBPA-AQ, the molecular orbital energy (E_{MO}) as a function of the fractional charge number (ΔN) in DBPA-AQ, ω^* and the absolute deviation of $E_{VA}(S_1)$ (AD) as functions of donor fragments, $E_{VA}(S_1)$ and $E_{VA}(T_1)$ as functions of the dielectric constant (ε), NTOs of S_1 and T_1 states with the corresponding weight of DMAC-Ph-AQ, training TADF molecules for establishing the r_{LOL}-ω^* relationship and comparison of the LOL and SLOL- and IP-tuning on the reproduction of the experimental ΔE_{ST}.

AUTHOR INFORMATION

Corresponding Author

* E-mail: chaowang89@zju.edu.cn and qishengzhang@zju.edu.cn

ACKNOWLEDGMENT

This work is supported by the Natural Science Foundation of China (Grant No. 51673164) and National Key R&D Program (Grant No. 2016YFB0401004).

REFERENCES

1. Baldo, M. A.; O'Brien, D. F.; Thompson, M. E.; Forrest, S. R., Excitonic Singlet-Triplet Ratio in a Semiconducting Organic Thin Film. *Phys. Rev. B* **1999**, *60*, 14422-14428.
2. Parker, C. A.; Hatchard, C. G., Triplet-Singlet Emission in Fluid Solutions. Phosphorescence of Eosin. *Transactions of the Faraday Society* **1961**, *57*, 1894.
3. Uoyama, H.; Goushi, K.; Shizu, K.; Nomura, H.; Adachi, C., Highly Efficient Organic Light-Emitting Diodes from Delayed Fluorescence. *Nature* **2012**, *492*, 234-238.
4. Lee, K.; Kim, D., Local-Excitation Versus Charge-Transfer Characters in the Triplet State: Theoretical Insight into the Singlet–Triplet Energy Differences of Carbazolyl-Phthalonitrile-Based Thermally Activated Delayed Fluorescence Materials. *J. Phys. Chem. C* **2016**, *120*, 28330-28336.
5. Samanta, P. K.; Kim, D.; Coropceanu, V.; Bredas, J. L., Up-Conversion Intersystem Crossing Rates in Organic Emitters for Thermally Activated Delayed Fluorescence: Impact of the Nature of Singlet Vs Triplet Excited States. *J. Am. Chem. Soc.* **2017**, *139*, 4042-4051.
6. Tao, Y.; Yuan, K.; Chen, T.; Xu, P.; Li, H.; Chen, R.; Zheng, C.; Zhang, L.; Huang, W., Thermally Activated Delayed Fluorescence Materials Towards the Breakthrough of Organoelectronics. *Adv. Mater.* **2014**, *26*, 7931-7958.
7. Moral, M.; Muccioli, L.; Son, W. J.; Olivier, Y.; Sancho-Garcia, J. C., Theoretical Rationalization of the Singlet-Triplet Gap in Oleds Materials: Impact of Charge-Transfer Character. *J. Chem. Theory Comput.* **2015**, *11*, 168-177.

8. Zhang, Q.; Li, J.; Shizu, K.; Huang, S.; Hirata, S.; Miyazaki, H.; Adachi, C., Design of Efficient Thermally Activated Delayed Fluorescence Materials for Pure Blue Organic Light Emitting Diodes. *J. Am. Chem. Soc.* **2012**, *134*, 14706-14709.

9. Zhang, Q.; Li, B.; Huang, S.; Nomura, H.; Tanaka, H.; Adachi, C., Efficient Blue Organic Light-Emitting Diodes Employing Thermally Activated Delayed Fluorescence. *Nat. Photonics* **2014**, *8*, 326-332.

10. Casida, M. E., Time-Dependent Density Functional Response Theory for Molecules. In *Recent Advances in Density Functional Methods (Part I)* Chong, D. P., Ed. World Scientific: Singapore, 1995; Vol. 1, pp 155-192.

11. Dreuw, A.; Weisman, J. L.; Head-Gordon, M., Long-Range Charge-Transfer Excited States in Time-Dependent Density Functional Theory Require Non-Local Exchange. *J. Chem. Phys.* **2003**, *119*, 2943-2946.

12. Casida, M. E.; Gutierrez, F.; Guan, J.; Gadea, F.-X.; Salahub, D.; Daudey, J.-P., Charge-Transfer Correction for Improved Time-Dependent Local Density Approximation Excited-State Potential Energy Curves: Analysis within the Two-Level Model with Illustration for H[Sub 2] and Lih. *J. Chem. Phys.* **2000**, *113*, 7062.

13. Rohrdanz, M. A.; Martins, K. M.; Herbert, J. M., A Long-Range-Corrected Density Functional That Performs Well for Both Ground-State Properties and Time-Dependent Density Functional Theory Excitation Energies, Including Charge-Transfer Excited States. *J. Chem. Phys.* **2009**, *130*, 054112.

14. Wang, C.; Yuan, Y.; Tian, X., Assessment of Range-Separated Exchange Functionals and Nonempirical Functional Tuning for Calculating the Static Second Hyperpolarizabilities of Streptocyanines. *J. Comput. Chem.* **2017**, *38*, 594-600.

15. Sun, H.; Zhong, C.; Bredas, J. L., Reliable Prediction with Tuned Range-Separated Functionals of the Singlet-Triplet Gap in Organic Emitters for Thermally Activated Delayed Fluorescence. *J. Chem. Theory Comput.* **2015**, *11*, 3851-3858.

16. Penfold, T. J., On Predicting the Excited-State Properties of Thermally Activated Delayed Fluorescence Emitters. *J. Phys. Chem. C* **2015**, *119*, 13535-13544.

17. Huang, S.; Zhang, Q.; Shiota, Y.; Nakagawa, T.; Kuwabara, K.; Yoshizawa, K.; Adachi, C., Computational Prediction for Singlet- and Triplet-Transition Energies of Charge-Transfer Compounds. *J. Chem. Theory Comput.* **2013**, *9*, 3872-3877.

18. Tian, X. H.; Sun, H. T.; Zhang, Q. S.; Adachi, C., Theoretical Predication for Transition Energies of Thermally Activated Delayed Fluorescence Molecules. *Chin. Chem. Lett.* **2016**, *27*, 1445-1452.

19. Wang, C.; Deng, C.; Wang, D.; Zhang, Q. S., Prediction of Intramolecular Charge-Transfer Excitation for Thermally Activated Delayed Fluorescence Molecules from a Descriptor-Tuned Density Functional. *J. Phys. Chem. C* **2018**, *122*, 7816-7823.

20. Le Bahers, T.; Adamo, C.; Ciofini, I., A Qualitative Index of Spatial Extent in Charge-Transfer Excitations. *J. Chem. Theory Comput.* **2011**, *7*, 2498-2506.

21. Guido, C. A.; Cortona, P.; Mennucci, B.; Adamo, C., On the Metric of Charge Transfer Molecular Excitations: A Simple Chemical Descriptor. *J. Chem. Theory Comput.* **2013**, *9*, 3118-3126.

22. Campetella, M.; Maschietto, F.; Frisch, M. J.; Scalmani, G.; Ciofini, I.; Adamo, C., Charge Transfer Excitations in Tddft: A Ghost-Hunter Index. *J. Comput. Chem.* **2017**, *38*, 2151-2156.

23. Wang, C.; Yuan, Y. Z.; Tian, X. H.; Yuan, J. Y.; Sun, J. Y., The Effect of Heteroatoms and End Groups of Polymethines on the All-Optical Switching Processing Application: A Cc2 Calculation. *Struct. Chem.* **2016**, *27*, 1211-1220.

24. Becke, A. D.; Edgecombe, K. E., A Simple Measure of Electron Localization in Atomic and Molecular Systems. *J. Chem. Phys.* **1990**, *92*, 5397-5403.

25. Schmider, H. L.; Becke, A. D., Chemical Content of the Kinetic Energy Density. *J. Mol. Struct.: THEOCHEM* **2000**, *527*, 51-61.

26. Savin, A.; Nesper, R.; Wengert, S.; Fässler, T. F., Elf: The Electron Localization Function. *Angew. Chem., Int. Ed.* **1997**, *36*, 1808-1832.

27. Wang, C.; Yuan, Y.; Tian, X.; Gieseking, R. L.; Sun, J., Recognition of Halides and Y-Shaped Oxoanions by Carbonylchromium-Based Urea-Like Molecules: A Theoretical Analysis of Hydrogen Bonding Modes. *J Mol Graph Model* **2016**, *64*, 1-10.

28. de Courcy, B.; Pedersen, L. G.; Parisel, O.; Gresh, N.; Silvi, B.; Pilme, J.; Piquemal, J. P., Understanding Selectivity of Hard and Soft Metal Cations within Biological Systems Using the Subvalence Concept. I. Application to Blood Coagulation: Direct Cation-Protein Electronic Effects Vs. Indirect Interactions through Water Networks. *J. Chem. Theory Comput.* **2010**, *6*, 1048-1063.

29. Becke, A. D., A New Inhomogeneity Parameter in Density-Functional Theory. *J. Chem. Phys.* **1998**, *109*, 2092-2098.
30. Borpuzari, M. P.; Kar, R., A New Nonempirical Tuning Scheme with Single Self-Consistent Field Calculation: Comparison with Global and Ip-Tuned Range-Separated Functional. *J. Comput. Chem.* **2017**, *38*, 2258-2267.
31. Fan, J.; Cai, L.; Lin, L.; Wang, C. K., Excited State Dynamics for Hybridized Local and Charge Transfer State Fluorescent Emitters with Aggregation-Induced Emission in the Solid Phase: A Qm/Mm Study. *Phys. Chem. Chem. Phys.* **2017**, *19*, 29872-29879.
32. Sun, H.; Hu, Z.; Zhong, C.; Chen, X.; Sun, Z.; Bredas, J. L., Impact of Dielectric Constant on the Singlet-Triplet Gap in Thermally Activated Delayed Fluorescence Materials. *J. Phys. Chem. Lett.* **2017**, *8*, 2393-2398.
33. Wang, H.; Xie, L.; Peng, Q.; Meng, L.; Wang, Y.; Yi, Y.; Wang, P., Novel Thermally Activated Delayed Fluorescence Materials-Thioxanthone Derivatives and Their Applications for Highly Efficient Oleds. *Adv. Mater.* **2014**, *26*, 5198-5204.
34. Zhang, Q.; Kuwabara, H.; Potscavage, W. J., Jr.; Huang, S.; Hatae, Y.; Shibata, T.; Adachi, C., Anthraquinone-Based Intramolecular Charge-Transfer Compounds: Computational Molecular Design, Thermally Activated Delayed Fluorescence, and Highly Efficient Red Electroluminescence. *J. Am. Chem. Soc.* **2014**, *136*, 18070-18081.
35. Cai, X.; Chen, D.; Gao, K.; Gan, L.; Yin, Q.; Qiao, Z.; Chen, Z.; Jiang, X.; Su, S.-J., “Trade-Off” Hidden in Condensed State Solvation: Multiradiative Channels Design for Highly Efficient Solution-Processed Purely Organic Electroluminescence at High Brightness. *Adv. Funct. Mater.* **2017**, 1704927.
36. Dos Santos, P. L.; Ward, J. S.; Bryce, M. R.; Monkman, A. P., Using Guest-Host Interactions to Optimize the Efficiency of Tadf Oleds. *J. Phys. Chem. Lett.* **2016**, *7*, 3341-3346.
37. Méhes, G.; Goushi, K.; Potscavage, W. J.; Adachi, C., Influence of Host Matrix on Thermally-Activated Delayed Fluorescence: Effects on Emission Lifetime, Photoluminescence Quantum Yield, and Device Performance. *Org. Electron.* **2014**, *15*, 2027-2037.

38. Tawada, Y.; Tsuneda, T.; Yanagisawa, S.; Yanai, T.; Hirao, K., A Long-Range-Corrected Time-Dependent Density Functional Theory. *J. Chem. Phys.* **2004**, *120*, 8425-8433.

39. Shimazaki, T.; Asai, Y., Band Structure Calculations Based on Screened Fock Exchange Method. *Chem. Phys. Lett.* **2008**, *466*, 91-94.

40. Refaely-Abramson, S.; Sharifzadeh, S.; Jain, M.; Baer, R.; Neaton, J. B.; Kronik, L., Gap Renormalization of Molecular Crystals from Density-Functional Theory. *Phys. Rev. B* **2013**, *88*.

41. Baer, R.; Livshits, E.; Salzner, U., Tuned Range-Separated Hybrids in Density Functional Theory. *Annu. Rev. Phys. Chem.* **2010**, *61*, 85-109.

42. Stein, T.; Kronik, L.; Baer, R., Reliable Prediction of Charge Transfer Excitations in Molecular Complexes Using Time-Dependent Density Functional Theory. *J. Am. Chem. Soc.* **2009**, *131*, 2818-2820.

43. Peach, M. J.; Williamson, M. J.; Tozer, D. J., Influence of Triplet Instabilities in Tddft. *J. Chem. Theory Comput.* **2011**, *7*, 3578-3585.

44. Sears, J. S.; Koerzdoerfer, T.; Zhang, C. R.; Bredas, J. L., Communication: Orbital Instabilities and Triplet States from Time-Dependent Density Functional Theory and Long-Range Corrected Functionals. *J. Chem. Phys.* **2011**, *135*, 151103.

45. Frisch, M. J.; Trucks, G. W.; Schlegel, H. B.; Scuseria, G. E.; Robb, M. A.; Cheeseman, J. R.; Scalmani, G.; Barone, V.; Petersson, G. A.; Nakatsuji, H., et al. *Gaussian 09*, D.01; Gaussian, Inc.: Wallingford CT, 2009.

46. Lu, T.; Chen, F., Multiwfn: A Multifunctional Wavefunction Analyzer. *J. Comput. Chem.* **2012**, *33*, 580-592.

47. Becke, A. D., Simulation of Delocalized Exchange by Local Density Functionals. *J. Chem. Phys.* **2000**, *112*, 4020-4026.

48. Korzdorfer, T.; Sears, J. S.; Sutton, C.; Bredas, J. L., Long-Range Corrected Hybrid Functionals for Pi-Conjugated Systems: Dependence of the Range-Separation Parameter on Conjugation Length. *J. Chem. Phys.* **2011**, *135*, 204107.

49. Pandey, L.; Doiron, C.; Sears, J. S.; Bredas, J. L., Lowest Excited States and Optical Absorption Spectra of Donor-Acceptor Copolymers for Organic Photovoltaics: A

New Picture Emerging from Tuned Long-Range Corrected Density Functionals. *Phys. Chem. Chem. Phys.* **2012**, *14*, 14243-14248.

50. Karolewski, A.; Stein, T.; Baer, R.; Kummel, S., Communication: Tailoring the Optical Gap in Light-Harvesting Molecules. *J. Chem. Phys.* **2011**, *134*, 151101.

51. Autschbach, J.; Srebro, M., Delocalization Error and "Functional Tuning" in Kohn-Sham Calculations of Molecular Properties. *Acc. Chem. Res.* **2014**, *47*, 2592-2602.

52. Mori-Sanchez, P.; Cohen, A. J.; Yang, W., Localization and Delocalization Errors in Density Functional Theory and Implications for Band-Gap Prediction. *Phys. Rev. Lett.* **2008**, *100*, 146401.

53. Janak, J. F., Proof That ∂E/∂N = Ei in Density-Functional Theory. *Phys. Rev. B* **1978**, *18*, 7165-7168.

54. Korzdorfer, T.; Parrish, R. M.; Sears, J. S.; Sherrill, C. D.; Bredas, J. L., On the Relationship between Bond-Length Alternation and Many-Electron Self-Interaction Error. *J. Chem. Phys.* **2012**, *137*, 124305.

55. Im, Y.; Kim, M.; Cho, Y. J.; Seo, J. A.; Yook, K. S.; Lee, J. Y., Molecular Design Strategy of Organic Thermally Activated Delayed Fluorescence Emitters. *Chem. Mater.* **2017**, *29*, 1946-1963.

56. Wong, M. Y.; Zysman-Colman, E., Purely Organic Thermally Activated Delayed Fluorescence Materials for Organic Light-Emitting Diodes. *Adv. Mater.* **2017**, *29*, 1605444.

57. Yang, Z.; Mao, Z.; Xie, Z.; Zhang, Y.; Liu, S.; Zhao, J.; Xu, J.; Chi, Z.; Aldred, M. P., Recent Advances in Organic Thermally Activated Delayed Fluorescence Materials. *Chem. Soc. Rev.* **2017**, *46*, 915-1016.

58. Zheng, Z.; Egger, D. A.; Bredas, J. L.; Kronik, L.; Coropceanu, V., Effect of Solid-State Polarization on Charge-Transfer Excitations and Transport Levels at Organic Interfaces from a Screened Range-Separated Hybrid Functional. *J. Phys. Chem. Lett.* **2017**, *8*, 3277-3283.

59. Northey, T.; Stacey, J.; Penfold, T. J., The Role of Solid State Solvation on the Charge Transfer State of a Thermally Activated Delayed Fluorescence Emitter. *J. Mater. Chem. C* **2017**, *5*, 11001-11009.

60. Fan, J. Z.; Lin, L. L.; Wang, C. K., Excited State Properties of Non-Doped Thermally Activated Delayed Fluorescence Emitters with Aggregation-Induced Emission: A Qm/Mm Study. *J. Mater. Chem. C* **2017**, *5*, 8390-8399.

61. de Silva, P.; Van Voorhis, T., Qm/Mm Study of Static and Dynamic Energetic Disorder in the Emission Layer of an Organic Light-Emitting Diode. *J. Phys. Chem. Lett.* **2018**, 1329-1334.

62. Kuang, Z. R.; He, G. Y.; Song, H. W.; Wang, X.; Hu, Z. B.; Sun, H. T.; Wan, Y.; Guo, Q. J.; Xia, A. D., Conformational Relaxation and Thermally Activated Delayed Fluorescence in Anthraquinone-Based Intramolecular Charge-Transfer Compound. *J. Phys. Chem. C* **2018**, *122*, 3727-3737.

63. Legaspi, C. M.; Stubbs, R. E.; Wahadoszaman, M.; Yaron, D. J.; Peteanu, L. A.; Kemboi, A.; Fossum, E.; Lu, Y.; Zheng, Q.; Rothberg, L. J., Rigidity and Polarity Effects on the Electronic Properties of Two Deep Blue Delayed Fluorescence Emitters. *J. Phys. Chem. C* **2018**, *122*, 11961-11972.

64. Wang, C.; Yuan, Y., The Influence of Aggregation on the Third-Order Nonlinear Optical Property of Pi-Conjugated Chromophores: The Case of Cyanine Dyes. *Phys. Chem. Chem. Phys.* **2018**, *20*, 16777-16785.

65. Liu, Z. T.; Kwong, C. Y.; Cheung, C. H.; Djurišić, A. B.; Chan, Y.; Chui, P. C., The Characterization of the Optical Functions of Bcp and Cbp Thin Films by Spectroscopic Ellipsometry. *Synth. Met.* **2005**, *150*, 159-163.

66. El‐Sayed, M. A., Spin–Orbit Coupling and the Radiationless Processes in Nitrogen Heterocyclics. *J. Chem. Phys.* **1963**, *38*, 2834-2838.

67. Marian, C. M., Spin-Orbit Coupling and Intersystem Crossing in Molecules. *WIREs Comput Mol Sci* **2012**, *2*, 187-203.

68. Gibson, J.; Monkman, A. P.; Penfold, T. J., The Importance of Vibronic Coupling for Efficient Reverse Intersystem Crossing in Thermally Activated Delayed Fluorescence Molecules. *Chemphyschem* **2016**, *17*, 2956-2961.

69. Chen, X. K.; Zhang, S. F.; Fan, J. X.; Ren, A. M., Nature of Highly Efficient Thermally Activated Delayed Fluorescence in Organic Light-Emitting Diode Emitters: Nonadiabatic Effect between Excited States. *J. Phys. Chem. C* **2015**, *119*, 9728-9733.

70. Etherington, M. K.; Gibson, J.; Higginbotham, H. F.; Penfold, T. J.; Monkman, A. P., Revealing the Spin-Vibronic Coupling Mechanism of Thermally Activated Delayed Fluorescence. *Nat Commun* **2016**, *7*, 13680.

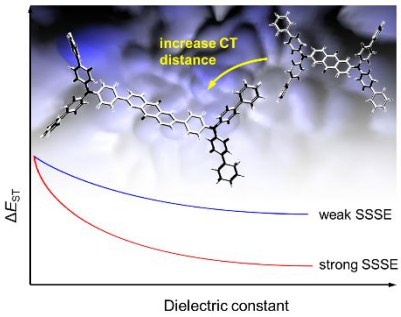
increase CT
distance
ΔE_{ST}
weak SSSE
strong SSSE
Dielectric constant

TOC Graphic

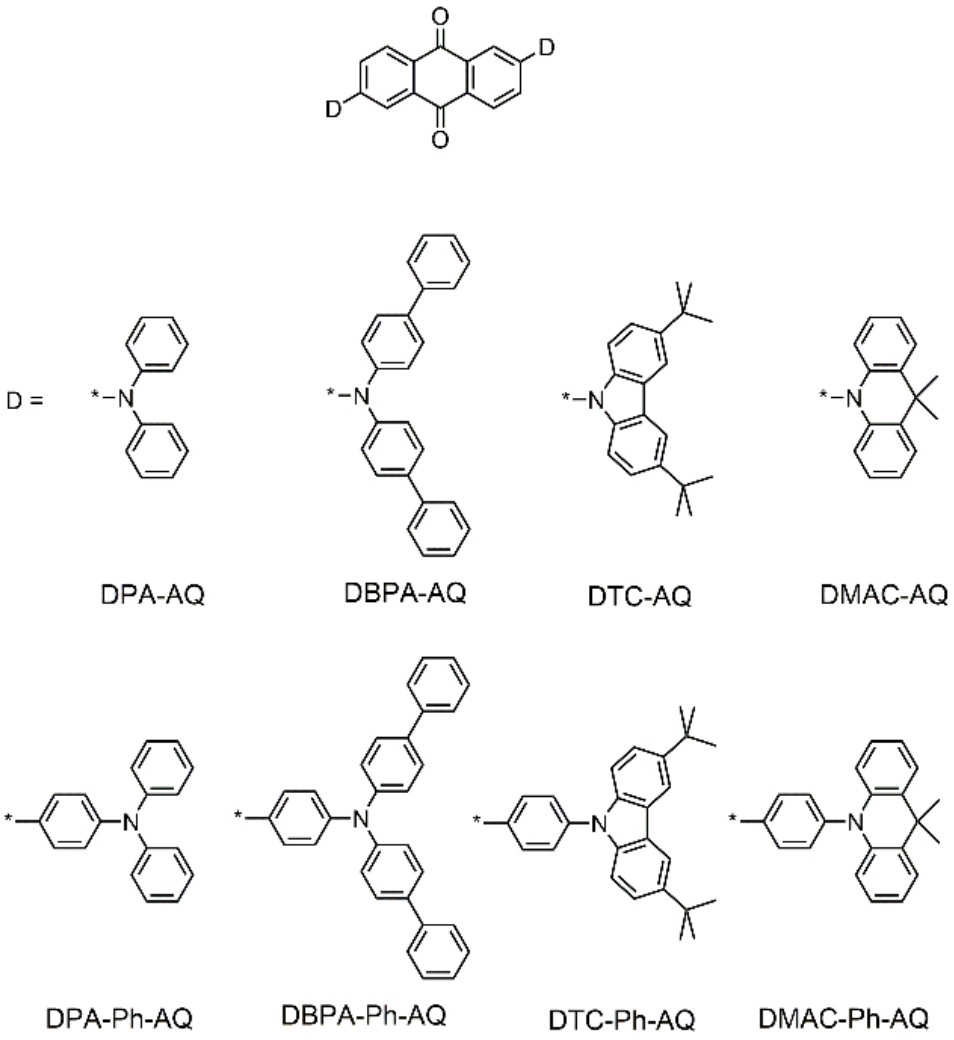

Figure 1

76x81mm (220 x 220 DPI)

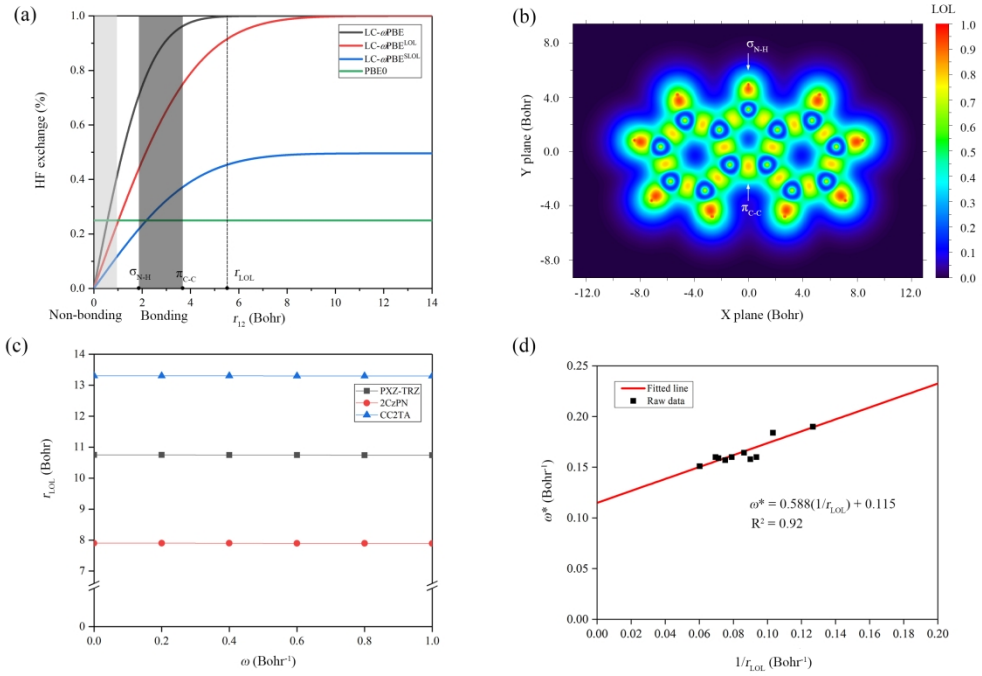
(a)
HF exchange (%)
LC-ωPBE
LC-ωPBE^LOL
LC-ωPBE^SLOL
PBE0
Non-bonding
Bonding
r12 (Bohr)
(b)
LOL
Y plane (Bohr)
X plane (Bohr)
(c)
PXZ-TRZ
2CzPN
CC2TA
ω (Bohr⁻¹)
(d)
Fitted line
Raw data
ω* = 0.588(1/r_LOL) + 0.115
R² = 0.92
1/r_LOL (Bohr⁻¹)

Figure 2

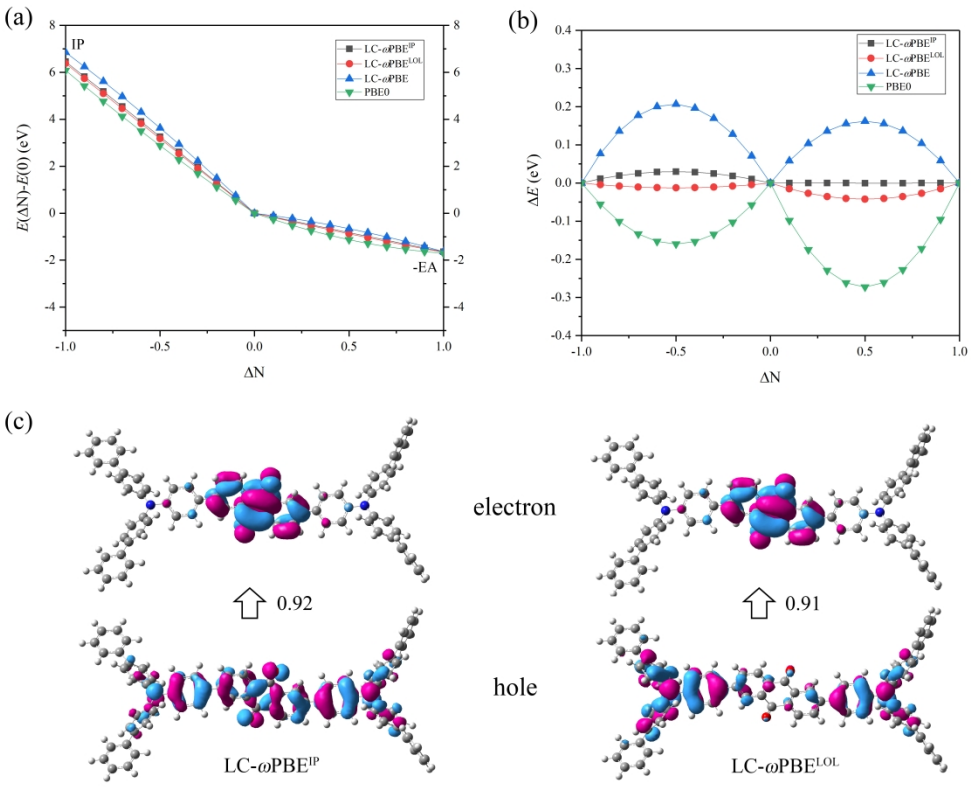

Figure 3

490x391mm (300 x 300 DPI)

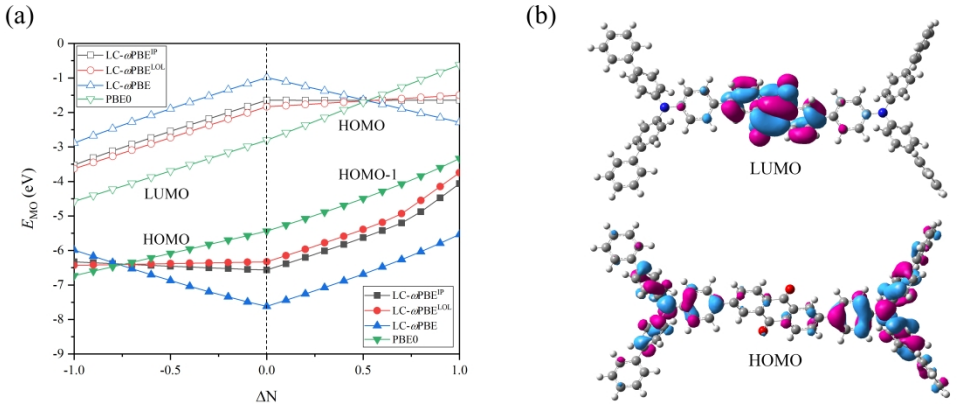

Figure 4

481x198mm (300 x 300 DPI)

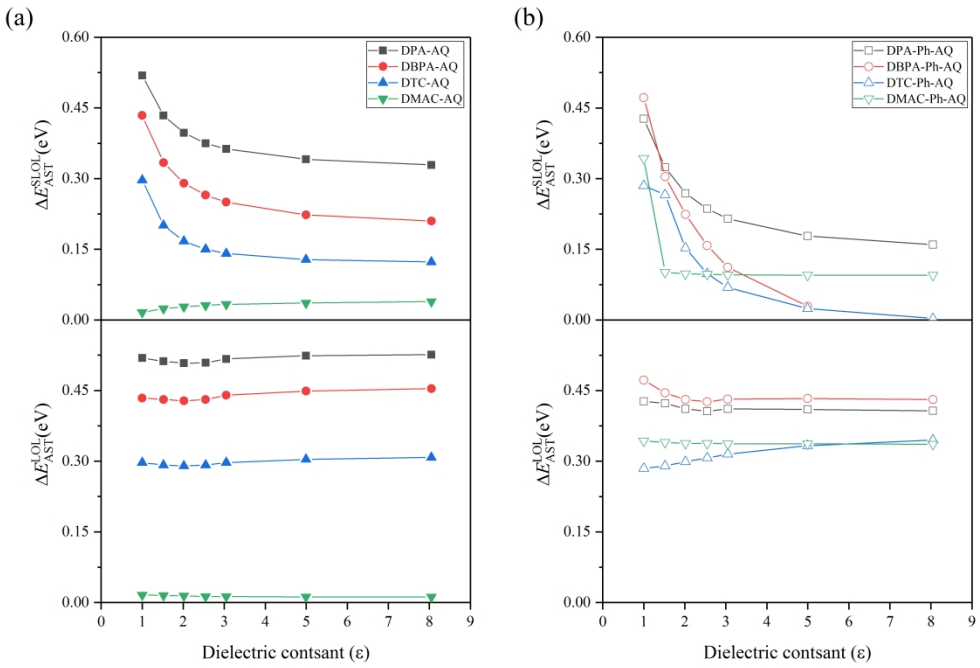
(a)
(b)
DPA-AQ
DBPA-AQ
DTC-AQ
DMAC-AQ
DPA-Ph-AQ
DBPA-Ph-AQ
DTC-Ph-AQ
DMAC-Ph-AQ
ΔE_{AST}^{SLOI}(eV)
ΔE_{AST}^{LOI}(eV)
Dielectric contsant (ε)

Figure 5

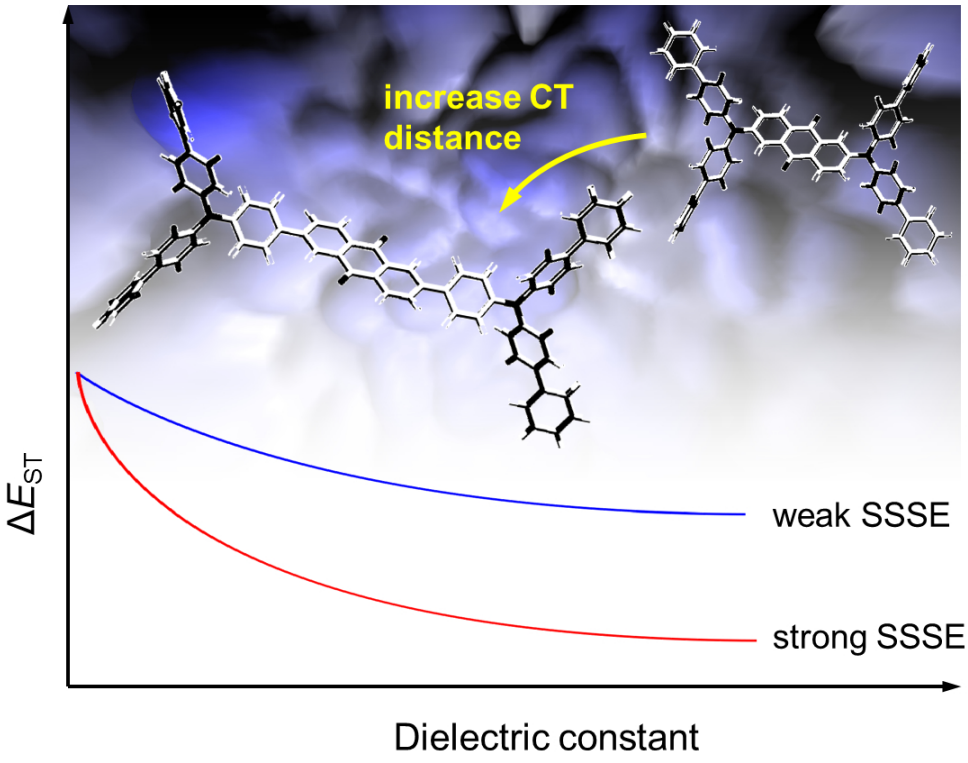

TOC

188x149mm (150 x 150 DPI)